Progress In Electromagnetics Research B, Vol. 66, 31–47, 2016

Analytical Model on Real Geometries of Magnet Bars of Surface Permanent Magnet Slotless Machine

Youcef Boutora[1, *], Noureddine Takorabet[2], and Rachid Ibtiouen[3]

Abstract—We present in this paper an analytical model for the calculation of the electromagnetic field in a slotless surface mounted permanent magnet machines. This model takes into account the two essential directions of magnetization of the magnets, namely tangential magnetization and radial magnetization. It especially accounts for the parallel form of the magnetization direction. The model uses equivalent currents on the surfaces of the magnets, and in an original way, it uses currents in all volume of the magnet. The model is validated by numerical results obtained with a free software of calculation of the electromagnetic fields (FEMM: Finite Element Method Magnetics) which uses the finite elements method and by an existing experimental structure. The model is extended to the magnets segmented in bars and separated. It is then extended to the shape of magnets close to parallepiped forms which are really used in large machines.

1. INTRODUCTION

The analytical field calculation has a large part in literature [1–24]. It provides exact results in fast time without numerical errors, like numerical methods. This is especially true when parameterized solutions have to be done requiring changes in machine dimension.

Since the availability of high energy product rare-earth permanent magnets, such as Samarium Cobalt (SmCo) in the 1970s and Neodymium Iron Boron (NdFeB) in the 1980s [3], the analytical calculation of the magnetic field in permanent-magnet-excited machines has received real interest in recent literature, and some methods were developed. One of these analytical methods is called the "subdomain" method and consists in solving directly the Maxwell's equations in the different subdomains, i.e., air-gap, stator slots and magnets, by the variables separation method [6, 7].

In magnetic field calculation of electrical permanent magnet machines, most authors consider a real direction of magnetization (parallel) [6–9, 24–28]. They consider only one permanent magnet by pole.

To optimize magnets on surface mounted machines to reduce cogging torque for example, many studies have been achieved to skewed magnets or slots, to consider magnet shifts and other solutions [4]. The influence of the type of magnetization (radial, radial parallel, shifted and Halbach magnets) is also taken into account in these models [3, 11, 12, 18, 19].

Boules [6] is one of the first authors who consider parallel magnetization in analytical field calculation for slotless surfaced mounted permanent magnet machines. He formulates a two-dimensional (2-D) model in polar coordinates that utilizes the concept of equivalent current-carrying coils to determine the airgap flux density distribution.

In [26], parallel magnets are given for surface mounted permanent magnet machines. The authors note that the model presented takes into account the interaction of the stator and rotor fields on drivers and thus determine the value of back electromotive forces (EMF).

Received 15 December 2015, Accepted 29 January 2016, Scheduled 12 February 2016

* Corresponding author: Youcef Boutora (yboutora@yahoo.fr).

[1] Laboratoire du Génie Electrique, Université Mouloud Mammeri BP17RP, Tizi-Ouzou 15000, Algeria. [2] Université de Lorraine GREEN, 2 Ave de la Forêt de Haye, 54516, France. [3] Laboratoire de Recherche en Electrotechnique, ENP 10, Ave Pasteur, BP, 182 El-Harrach, Algiers 16200, Algeria.

In [27], an experimental study is achieved on BDLC with two types of magnetizations: radial and parallel magnetization. The authors compare the performance of a BLDC machine with radial magnet and parallel magnets. He note that the parallel magnetization induces a lower cogging torque but greater hysteresis loss.

Authors of [28] consider that the parallel magnetization is easier to obtain for the radial magnetization tiles. More they note that the parallel magnetization induces iron losses slightly larger than the radial magnetization. However, they also note that the total power required for radial magnetized machine is slightly greater than for the parallel machine with the same operating torque and speed. The authors conclude that for the choice of the type of magnetization, it is more advisable and easier to adopt the parallel magnetization process when the magnets are subjected to the action before the magnetization introduction in the motor, as it is verified in a wide number of applications.

We can see that parallel magnetization has many advantages compared to radial magnetization: easier to perform, less cogging torque, and comparable efficiency for radial magnetization machines.

An analytical model of parallel permanent and radial magnets in slotted stator machines is presented in [8]. We can consider this work as a result of a previous work given in [7]. The magnetization is supposed constant in all permanent magnets. Variable separation method is used to solve the partial differential equation in all domains. Algebraic linear equations are taken to find some constants related to magnetic field.

This method is also applied in some papers [11–18] for slotted stator in permanent magnet machine (surface mounted permanent magnet machines, inset permanent magnet machines...).

In [21], to perform optimum magnet pole shape design for the reduction of torque ripple, authors consider the special geometrical form of magnets.

In the design, generally, a set of magnet bars is used under one pole. Each magnet bar has its parallel direction of magnetization. It is hard to optimize these machines in terms of number of magnet bars, under mechanical considerations.

In this paper, we present a complete model of permanent magnet bars with parallel magnetization. We not only use surface equivalent currents for modeling permanent magnets, but also introduce volume currents in the case of parallel magnetization. The presented model permits to directly determine the fundamental of spatial magnetic field distribution and all harmonics, and their variations versus number of magnet bars. It is then possible to perform the design of structures if we consider air gap flux density as reference.

On the other hand, in addition to previous works, we are also interest in tangential and parallel tangential permanent magnet structures. These types of magnetization (in [29], we have tangential magnetization component which exists in practice in a multipole impulse magnetized isotropic ring PM) are present in combined magnetization segment bars, as shifted and Halbach structures.

The model, which is applied at first (in all this study) to a slotless structure, is extended to segmented permanent magnet bars and separate segmented PMs. An equivalent model to parallelepiped magnet bars in both magnetizations (radial parallel and tangential parallel) is also given in this paper.

The obtained model is applied to a laboratory slotless surface permanent machine. Experimental results are presented [22, 23] and compared with analytical model. For validation of the presented model in other cases, we replace, for the same structure, the magnets with considering both radial and tangential magnetization in parallel and axial directions.

2. PERMANENT MAGNET MACHINE MODEL

2.1. Model Assumptions

At first, we consider 2-D model in polar coordinates. Then we consider only (r, θ) components. We suppose then an invariance of flux density in z coordinate.

Stator and rotor laminations are supposed to have infinite permeability ($\mu_s \approx \infty$). It is possible if we consider that iron steel used in stator and rotor have a permeability which is largely most important than airgap and magnet permeabilities. The relative permeability of the magnets is supposed to be equal to 1 as for the air-gap. It is available for advanced permanent magnets such as Nd-Fe-B and Sm-Co ($\mu_r \approx 1.015$ to 1.2).

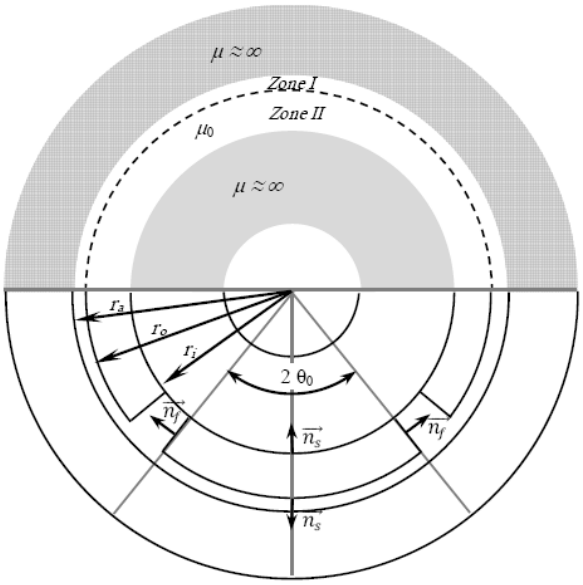

Figure 1. Structure of surface mounted permanent magnet machine with slotless stator.

Another assumption concerns permanent magnet used in this study and shown in Fig. 1. We can see that there are two parts: iron part and air part.

The air part consists of mechanical air gap (zone I) and permanent magnet zone (zone II). This part is also called magnetic air gap.

Permanent magnets are mounted on rotor in zone II. They are surrounded by two types of surfaces: external and frontal surfaces. Normal vectors are represented on magnets (Fig. 1).

$\vec{n}_s$ for external surfaces

$\vec{n}_f$ for frontal surfaces

The inner radius of the rotor is given by r_i and its outer radius given by r_o. Inner radius of the stator is designed by r_a. The machine has $2p$ poles.

The electrical shift of permanent magnets is $2 \times \theta_o$. This shift includes all segmented bars of the permanent magnet. We consider n_b bars for each permanent magnet.

2.2. One Bar Permanent Magnet Model

The proposed model of the magnets consists of a magnetic polarization vector which varies according to its radius:

$$M = \mu_0 M_0 \frac{r_m}{r} \tag{1}$$

With $r_m = \frac{r_o - r_i}{2}$.

M_0 is the given magnetization value of permanent magnet.

Classical models (radial and tangential) and parallel models of permanent magnets are represented in Fig. 2.

In classical cases, we have only surface currents: external surface currents for tangential magnetization and frontal surface currents for radial magnetization.

Magnetization vector is written by Eq. (2) for tangential case, by Eq. (3) for radial case, by Eq. (4) for tangential parallel case and by Eq. (5) for radial parallel case

$$\overrightarrow{M_t} = 0\overrightarrow{u_r} + M \cdot \overrightarrow{u_\theta} \tag{2}$$

$$\overrightarrow{M_r} = M\overrightarrow{u_r} + 0 \cdot \overrightarrow{u_\theta} \tag{3}$$

$$\overrightarrow{M_{tp}} = M \cdot \sin\theta\overrightarrow{u_r} + M \cdot \cos\theta\overrightarrow{u_\theta} \tag{4}$$

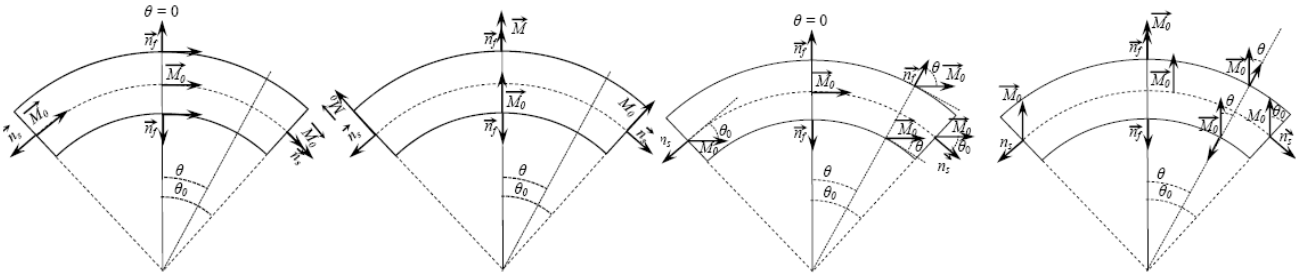

(a) (b) (c) (d)

Figure 2. Models of permanents magnets models in magnetization. (a) Tangential. (b) Radial. (c) Tangential parallel. (d) Radial parallel.

$$\overrightarrow{M_{rp}} = M \cdot \cos\theta \overrightarrow{u_r} - M \cdot \sin\theta \overrightarrow{u_\theta} \tag{5}$$

Equivalent currents are alternative and can be expressed by a development of Fourier series.

2.3. Equivalent Currents for Model Magnets in Fourier Series

1. Surface currents:

Adopting Amperian equivalent model, we can estimate equivalent currents in all the volume of permanent magnet with its surfaces.

For surface currents, we have: $\overrightarrow{Js} = \vec{M} \times \vec{n}_s$.

We have then, respectively for Eqs. (2), (3), (4) and (5):

$$\overrightarrow{Js_t} = M \cdot \vec{k} \tag{6}$$

$$\overrightarrow{Js_r} = 0 \tag{7}$$

$$\overrightarrow{Js_{tp}} = \pm M \cos\theta \vec{k} \tag{8}$$

$$\overrightarrow{Js_{rp}} = \pm M \sin\theta \vec{k} \tag{9}$$

We note that the surface currents in the case of a radial magnetization are zero.

For frontal surface currents, we have: $\overrightarrow{J_f} = \vec{M} \times \vec{n}_f$ and then respectively for Eqs. (2), (3), (4) and (5). In these cases, we consider frontal equivalent currents localized in points at θ_0 and θ_0. We can then use the Dirac function.

$$\overrightarrow{Jf_t} = 0 \tag{10}$$

$$\overrightarrow{Jf_r} = \frac{M}{r} \cdot \vec{k} \tag{11}$$

$$\overrightarrow{Jf_{tp}} = \pm \frac{M}{r} \sin\theta_0 \vec{k} \tag{12}$$

$$\overrightarrow{Jf_{rp}} = \pm \frac{M}{r} \cos\theta_0 \vec{k} \tag{13}$$

2. Volume currents

Originality of this work consists in introducing volume currents. The surface currents model is insufficient to represent the complete model of permanent magnets. These currents are obtained with the expression: $\overrightarrow{J_v} = \overrightarrow{curl}\vec{M}$.

We have then volume currents obtained in Eqs. (14), (15), (16) and (17) for magnetization given in Eqs. (2), (3), (4) and (6).

$$\overrightarrow{Jv_t} = 0 \tag{14}$$

$$\overrightarrow{Jv_r} = 0 \tag{15}$$

$$\overrightarrow{Jv_{tp}} = \frac{M}{r} \cos\theta \vec{k} \tag{16}$$

$$\overrightarrow{Jv_{rp}} = \frac{M}{r}\sin\theta\vec{k} \tag{17}$$

For classical models (tangential and radial), volume currents are equal to zero, contrary to parallel magnetization.

2.4. Fourier Series Currents

The sum of all currents (surface J_s, frontal J_f and volume J_v) gives all source currents to Amperian model for each magnetization type.

Then we have, respectively for tangential, radial, tangential parallel and radial parallel Equations (18), (19), (20) and (21)

$$\overrightarrow{J_t} = M \cdot \vec{k} \tag{18}$$

$$\overrightarrow{J_r} = \pm\frac{M}{r}\delta_{\theta_0} \cdot \vec{k} \tag{19}$$

$$\overrightarrow{J_{tp}} = \left(\pm M\cos\theta + \frac{M}{r}\left(\pm\sin\theta_0\delta_{\theta_0} + \cos\theta\right)\right)\vec{k} \tag{20}$$

$$\overrightarrow{J_{rp}} = \left(\pm M\sin\theta + \frac{M}{r}\left(\pm\cos\theta_0\delta_{\theta_0} + \sin\theta\right)\right)\vec{k} \tag{21}$$

In Fourier series, equivalent current of the models expressed in Eqs. (2), (3), (4) and (5) are given respectively by Eqs. (22), (23), (24) and (25).

$$J_t(\theta) = \pm M\frac{4p}{\pi}\sum_k \sin\left(n\theta_0\right)\cos\left(n\theta\right) \tag{22}$$

$$J_r(\theta) = -\frac{M}{r}\frac{4p}{\pi}\sum_k \sin\left(n\theta_0\right)\sin\left(n\theta\right) \tag{23}$$

$$J_{tp}(\theta) = M\sum_k \left(S_{tk} + \frac{4p}{\pi}\frac{1}{r}\sin\theta_0\cos\left(n\theta_0\right) + \frac{1}{r}S_{tk}\right)\cos\left(n\theta\right) \tag{24}$$

$$J_{rp}(\theta) = M\sum_k \left(S_{rk} + \frac{4p}{\pi}\frac{1}{r}\cos\theta_0\sin\left(n\theta_0\right) + \frac{1}{r}S_{rk}\right)\sin\left(n\theta\right) \tag{25}$$

With $n = (2k+1)p$

$$S_{t_k} = \begin{cases} \dfrac{1}{\pi}\left(2\theta_0 + \sin\left(2\theta_0\right)\right) & n = 1 \\ \dfrac{2p}{\pi}\left(\dfrac{\sin\left(n-1\right)\theta_0}{(n-1)} + \dfrac{\sin\left(n+1\right)\theta_0}{(n+1)}\right) & n \neq 1 \end{cases} \tag{26}$$

And

$$S_{r_k} = \begin{cases} \dfrac{1}{\pi}\left(2\theta_0 - \sin\left(2\theta_0\right)\right) & n = 1 \\ \dfrac{2p}{\pi}\left(\dfrac{\sin\left(n-1\right)\theta_0}{(n-1)} - \dfrac{\sin\left(n+1\right)\theta_0}{(n+1)}\right) & n \neq 1 \end{cases} \tag{27}$$

3. SEGMENTED MAGNET BARS MODEL

The developed model is now applied to the segmented magnets. Each tile consists of n_b bars whose magnetizing is located according to the axis of each of these bars. It is supposed that all bars are identical under each pole (even angle shift, even thickness, even value of magnetization).

Each ith bar is located at the angle θ_i as this:

$$\theta_i = -\theta_0 + (2i-1)\,\theta_b \tag{28}$$

$$\theta_b = \frac{\theta_0}{n_b} \tag{29}$$

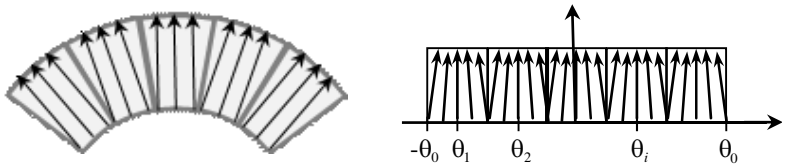

Figure 3. Permanent magnet structured in bars.

The magnetization vector is given by Eq. (30) for segmented radial parallel tiles and by Eq. (31) for segmented tangential parallel tiles.

$$\overrightarrow{M_i} = M \cdot \cos(\theta - \theta_i)\,\overrightarrow{u_r} - M \cdot \sin(\theta - \theta_i)\,\overrightarrow{u_\theta} \tag{30}$$

$$\overrightarrow{M_i} = M \cdot \sin(\theta - \theta_i)\,\overrightarrow{u_r} + M \cdot \cos(\theta - \theta_i)\,\overrightarrow{u_\theta} \tag{31}$$

For surface currents, we have Eq. (32) for segmented radial parallel tiles and Eq. (33) for segmented tangential parallel tiles.

$$\mu_0 J_s = \left(\sum_{i=1}^{n_b} \mu_0 S_{kr_i}\right) \sin n\theta \tag{32}$$

$$\mu_0 J_s(\theta) = \left(\sum_{k}\sum_{i=1}^{n_b} \mu_0 S_{kt_i}\right) \cos n\theta \tag{33}$$

For frontal surface currents, we have Eq. (34) for segmented radial parallel tiles and Eq. (35) for segmented tangential parallel tiles.

$$\mu_0 J_r = \mu_0 \Re_{kr} \sin n\theta \tag{34}$$

$$\mu_0 J_r = \mu_0 \sum_{k} \Re_{kt} \cos n\theta \tag{35}$$

For volume surface currents, we have Eq. (36) for segmented radial parallel tiles and Eq. (37) for segmented tangential parallel tiles.

$$\mu_0 J_v = \frac{\mu_0}{r} \sum_{k} S_{kr_i} \sin n\theta \tag{36}$$

$$\mu_0 J_v(r,\theta) = \mu_0 \sum_{k}\sum_{i=1}^{n_b} \frac{S_{kt_i}}{r} \cos(2k+1)p\theta \tag{37}$$

With

$$\mu_0 S_{kt_i} = \begin{cases} M_0 \dfrac{r_m}{\pi r} \cos\theta_i \left(2\theta_b - \sin(2\theta_b)\right) & n = 1 \\ M_0 \dfrac{r_m}{\pi r} 2p \cos(n\theta_i) \left(\dfrac{\sin(n-1)\,\theta_b}{(n-1)} - \dfrac{\sin(n+1)\,\theta_b}{(n+1)}\right) & n \neq 1 \end{cases} \tag{38}$$

$$\mu_0 S_{kt_i} = \begin{cases} M_0 \dfrac{r_m}{\pi r} \cos\theta_i \left(2\theta_b + \sin(2\theta_b)\right) & n = 1 \\ M_0 \dfrac{r_m}{\pi r} 2p \cos(n\theta_i) \left(\dfrac{\sin(n-1)\,\theta_b}{(n-1)} + \dfrac{\sin(n+1)\,\theta_b}{(n+1)}\right) & n \neq 1 \end{cases} \tag{39}$$

$$\mu_0 \Re_{kr} = 4p \frac{M \cdot r_m}{\pi r^2} \sin n\theta_0 \cos\theta_b \tag{40}$$

$$\mu_0 \Re_{kt} = 4p \frac{M \cdot r_m}{\pi r^2} \sin\theta_b \cos n\theta_0 \sum_{i=1}^{n_b} \cos n\theta_i \tag{41}$$

4. SEGMENTED PARALLELEPIPED BARS

In practice, the magnet bars are parallepipedic. The presented model takes account of magnets in a tile form. We propose an analytical model that takes into account equivalent appearance parallelepiped magnets.

As shown in Fig. 4, the parallepiped magnet is defined with two angles:

- Maximum angle which is on the iron core; its value is done by $2 \times \theta_b$.
- Equivalent angle which is given by $2 \times \alpha \times \theta_b$ (Fig. 4).

α is calculated as following:

$$\alpha = \frac{1}{\theta_b} \arctan \left(2 \frac{r_i \sin \theta_b}{\left(r_o^2 - r_i^2 \sin^2 \theta_b\right)^{\frac{1}{2}} + r_i \cos \theta_b} \right) \tag{42}$$

α depends, for the studied structure, on p (number of pair poles) and number of segmented bars by pôle.

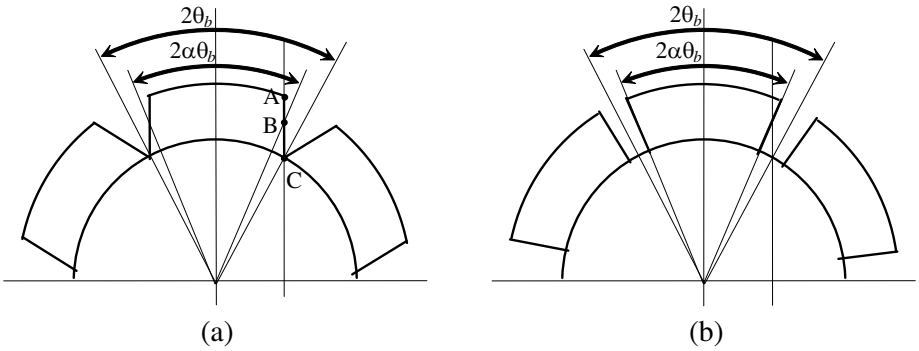

Figure 4. Equivalent model of real magnet segmented bars. (a) Pseudo-parallepiped magnets. (b) Tile magnets.

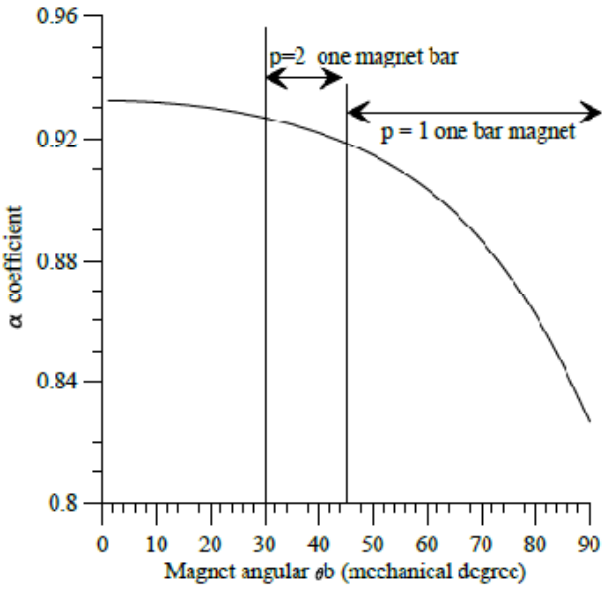

Figure 5. Variations of α versus θ_b.

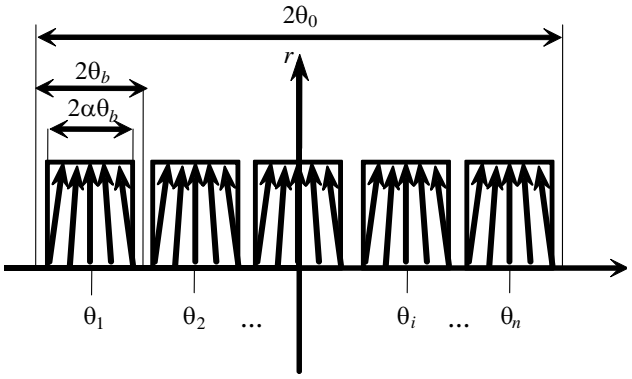

Figure 6. Analytical model of separated parallel magnet bars.

Figure 5 shows α variations versus θ_b angle of magnets.

If we consider that magnet bars have a half open angle less than 30° (in mechanical degrees), then α coefficient varies between 0.927 and 0.932. For all suitable study, α coefficient is calculated for each configuration.

In this model, we consider the parallel magnet bars as separated with $2\theta_b$ angular shift, but for parallepipedic magnets, they have a reduced angular shift of $2\alpha\theta_b$ (see Fig. 6). We consider two types of magnetization: radial parallel and tangential parallel.

1. Radial parallel magnetization

a. Internal external Surface currents

$$\mu_0 J_s(\theta) = \left(\sum_k \sum_{i=1}^{n_b} \mu_0 S_{k_i} \right) \sin n\theta \tag{43}$$

$$S_{k_i} = \begin{cases} M_0 \dfrac{r_m}{\pi r} \cos\theta_i \left(2\alpha\theta_b - \sin\left(2\alpha\theta_b\right)\right) & n = 1 \\ M_0 \dfrac{r_m}{\pi r} 2p \cos\left(n\theta_i\right) \left(\dfrac{\sin\left(n-1\right)\alpha\theta_b}{(n-1)} - \dfrac{\sin\left(n+1\right)\alpha\theta_b}{(n+1)} \right) & n \neq 1 \end{cases} \tag{44}$$

b. Frontal surface currents

$$\mu_0 J_r = \mu_0 \sum_k \Re_k \sin n\theta \tag{45}$$

$$\Re_k = 4p \frac{M \cdot r_m}{\pi r^2} \cos\left(\alpha\theta_b\right) \sum_{i=1}^{n_b} \sin\left(n\left(\theta_i - \alpha\theta_b\right)\right) \tag{46}$$

with $\theta_i = (-n_b + 2i - 1)\theta_b$.

c. Volume currents:

$$\mu_0 J_v(r,\theta) = \mu_0 \sum_k \sum_{i=1}^{n_b} \frac{S_{k_i}}{r} \sin n\theta \tag{47}$$

2.Tangential parallel magnetization

For internal and external surface, the equivalent current is:

$$\mu_0 J_s(\theta) \left(\sum_k \sum_{i=1}^{n_b} \mu_0 S_{k_i} \right) \cos n\theta \tag{48}$$

$$S_{k_i} = \begin{cases} M_0 \dfrac{r_m}{\pi r} \cos\theta_i \left(2\alpha\theta_b + \sin\left(2\alpha\theta_b\right)\right) & n = 1 \\ M_0 \dfrac{r_m}{\pi r} 2p \cos\left(n\theta_i\right) \left(\dfrac{\sin\left(n-1\right)\alpha\theta_b}{(n-1)} + \dfrac{\sin\left(n+1\right)\alpha\theta_b}{(n+1)} \right) & n \neq 1 \end{cases} \tag{49}$$

For the frontal surfaces, the equivalent current is:

$$\mu_0 J_r = \mu_0 \sum_k \Re_k \cos n\theta \tag{50}$$

$$\Re_k = 4p \frac{M \cdot r_m}{\pi r^2} \sin\left(\alpha\theta_b\right) \cos\left(n\alpha\theta_b\right) \sum_{i=1}^{n_b} \cos n\theta_i \tag{51}$$

Inside the magnets, we have volume currents:

$$\mu_0 J_v(r,\theta) = \mu_0 \sum_k \sum_{i=1}^{n_b} \frac{S_{k_i}}{r} \cos n\theta \tag{52}$$

5. POTENTIAL MAGNETIC VECTOR

We solve a partial differential equation in polar coordinates (r, θ) in potential vector formulation only in magnetic air gap. The potential vector A (the scalar value of the z-component of magnetic potential vector) is calculated separately for each component of equivalent currents of permanent magnets (external current surfaces, frontal current surfaces and volume currents). All calculated potentials are added to obtain final result.

For external currents surface, we solve Poisson's equation in all magnetic air gaps and consider Equation (53):

$$\Delta A = \frac{\partial^2}{\partial r^2}A + \frac{1}{r}\frac{\partial}{\partial \theta}A + \frac{\partial^2}{\partial \theta^2}A = 0 \tag{53}$$

For frontal currents surface and volume currents, we solve Laplace's equation and consider Equation (54):

$$\Delta A = \frac{\partial^2}{\partial r^2}A + \frac{1}{r}\frac{\partial}{\partial \theta}A + \frac{\partial^2}{\partial \theta^2}A = \mu_o J \tag{54}$$

J is the total equivalent current of permanent magnet.

Polar components of flux density vector B are given by:

$$\vec{B} = \overrightarrow{curl}\vec{A} = \frac{1}{r}\frac{\partial A}{\partial \theta}\vec{u}_r - \frac{\partial A}{\partial r}\vec{u}_\theta = B_r\vec{u}_r + B_\theta\vec{u}_\theta \tag{55}$$

We consider the separate variables method to solve the partial differential equations. Then, we consider potential magnetic A as the product of two functions:

$$A(r,\theta) = R(r)\cdot\Theta(\theta) \tag{56}$$

$R(r)$ is a function that depends only on r, and $\Theta(\theta)$ is a function that depends only on θ.

6. APPLICATION ON A REAL STRUCTURE

We take the structure described in Table 1 [22, 23] and Fig. 7. It is a machine prototype developed by the Laboratory LEEI Toulouse (France). It is a machine with six poles ($p = 3$). Each pole is occupied by two radial parallel magnets ($n_b = 2$). A search coil is inserted in the air gap of the machine driven by a gear motor with low variable speed. Experimental results concerning normal flux density in the air gap are given in Fig. 8(a). Analytical and FEMM results are given in Fig. 8(b). A good correlation is observed among all these results. We can conclude that for this structure the proposed model is valid.

Table 1. Characteristics of studied slotless permanent machine.

External radius (mm)	125.5
Inner radius of rotor r_i (mm)	69
Outer radius of rotor r_o (mm)	79
Inner radius of stator r_a (mm)	87
Magnetization $M(T)$	0.9
Mechanical airgap (mm)	3
Number of bars n_b	2
Number of poles $2p$	6

1. Radial parallel permanent magnet bars

We use finite elements results to provide a freeware tool, which is FEMM 4.2 (finite elements method magnetics) [30]. The numerical model solves magnetostatic equation in a Cartesian coordinates. With a compiled Lua program, we compute the geometric structures with real forms (in linear case) at no load. We fixed permanent magnet relative permeability at 1 and iron (stator and rotor) permeability at 1000.

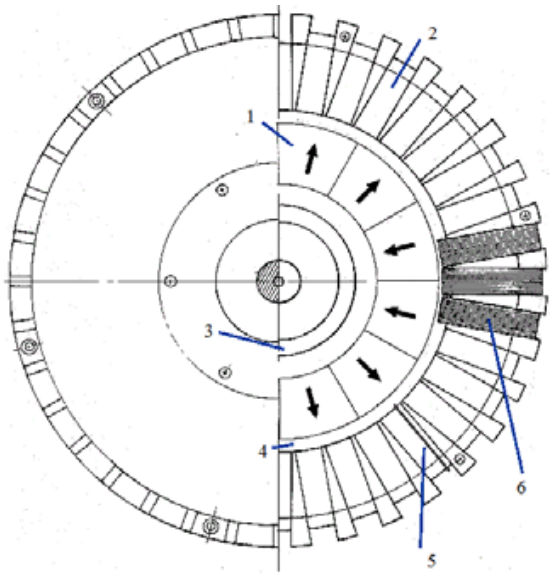

Figure 7. Real structure for experiments. 1. Permanent magnets. 2. Stator yoke. 3. Rotor yoke. 4. Airgap. 5. Search coil. 6. Stator windings.

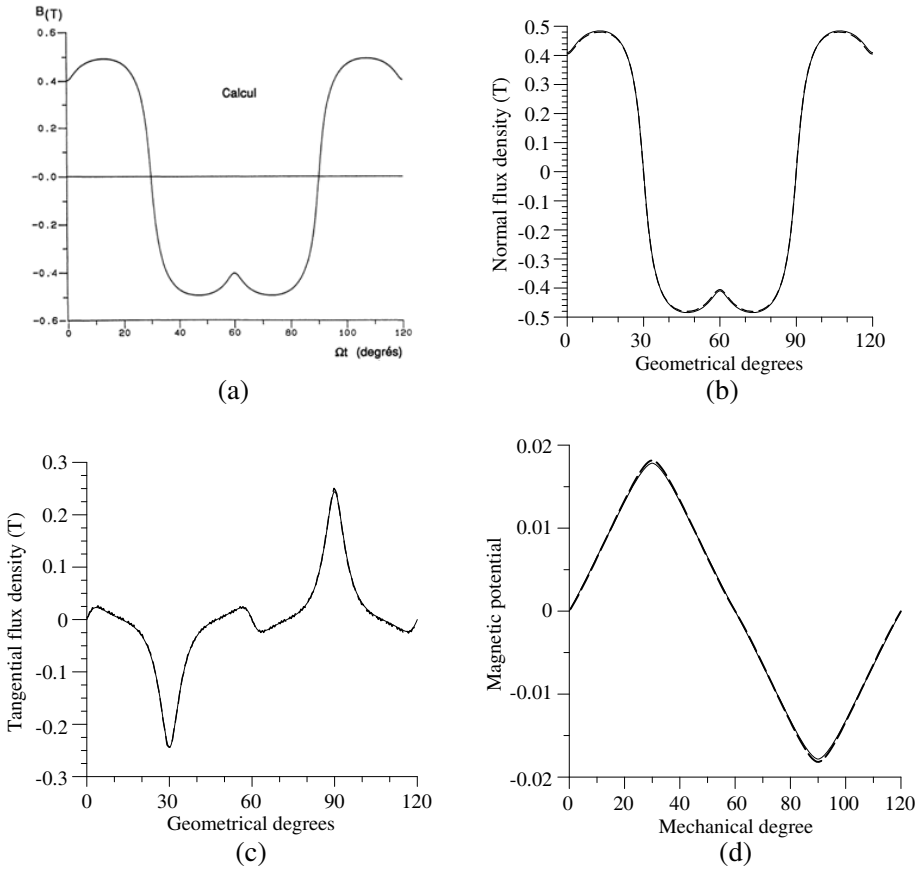

Figure 8. Finite element model (– – –) and analytical model (——) comparison of tangential component of flux density and potential. (a) Experiments [21]. (b) Numerical (– – –) and model calculation (——). (c) Tangential component of flux density. (d) Potential.

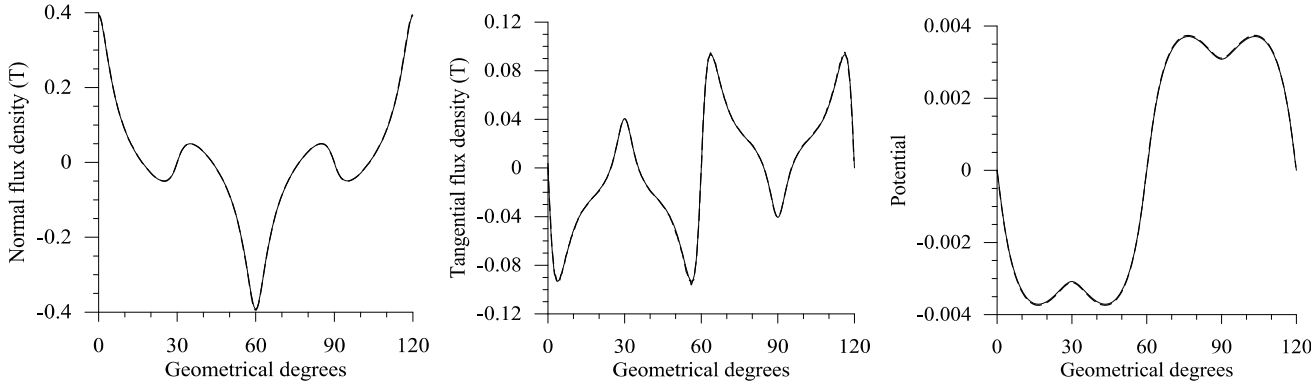

Figure 9. Finite element model (– – –) and analytical model (——) comparison of radial component of flux density for parallel tangential magnetization.

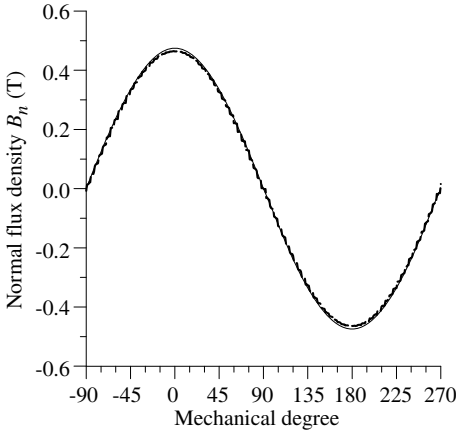

Figure 10. Bipolar machine with total shift of permanent magnets $\theta_0 = 90°$ (—— analytical model) and (– – – finite elements model).

Analytical calculation of tangential component of flux density is also given with FEMM calculation in Fig. 8(a). A very good correlation is also noticed in this case. The developed model is then correct for this structure. In Fig. 8(b), we can see potential results for both analytical and FEMM results.

For tangential parallel magnetization, we suppose the same structure studied for radial parallel magnetization and change only the type of magnetization of magnet bars.

Then we have both analytical and FEMM results for normal and tangential components of flux density in air gap, and the potential values (see Fig. 9).

In Fig. 10, we can see a normal flux density component for a complete shifting of permanent magnets ($\theta_0 = 90°$). Each permanent magnet covers the whole pole of the machine. The normal flux density is a perfect sine wave in this case. This result is confirmed by many researches in literature. We can see that developed model results are the same as FEMM.

In this case, equivalent frontal currents equal zero, and other currents (surface and volume) are in only the first term of Series Fourier transform. Equations (12) and (16) for tangential parallel magnetization and (13) and (17) for radial parallel magnetization will be respectively Eqs. (57) and (58).

$$J_{tp}(\theta) = M\left(1 + \frac{1}{r}\right)\cos(\theta) \tag{57}$$

$$J_{rp}(\theta) = M\left(1 + \frac{1}{r}\right)\sin(\theta) \tag{58}$$

In Fig. 11(a), the 2-pole structure is studied with approached 2/3 shift permanent magnet

($\theta_0 = 60°$). Also in this case, analytical and FEMM results are the same. We have decomposed normal components of flux density with the contributions of all types of currents modeled permanent magnets. In this case, we can see that the contributions of volume currents and frontal surface currents are the same (in maximum value). It is a particular case.

Internal and external surface currents have a little contribution, and their principal effects are at the ends of magnets. It has a negative effect. It is opposed to the other types of currents. In the middle of the magnets, internal-external currents has a small contribution.

In Fig. 11(b), we can see related contribution of all type of equivalent currents in the maximum value of normal flux density. Total normal flux density is related to 100%.

As we can see, volume currents contribution are increased when the length of permanent magnets

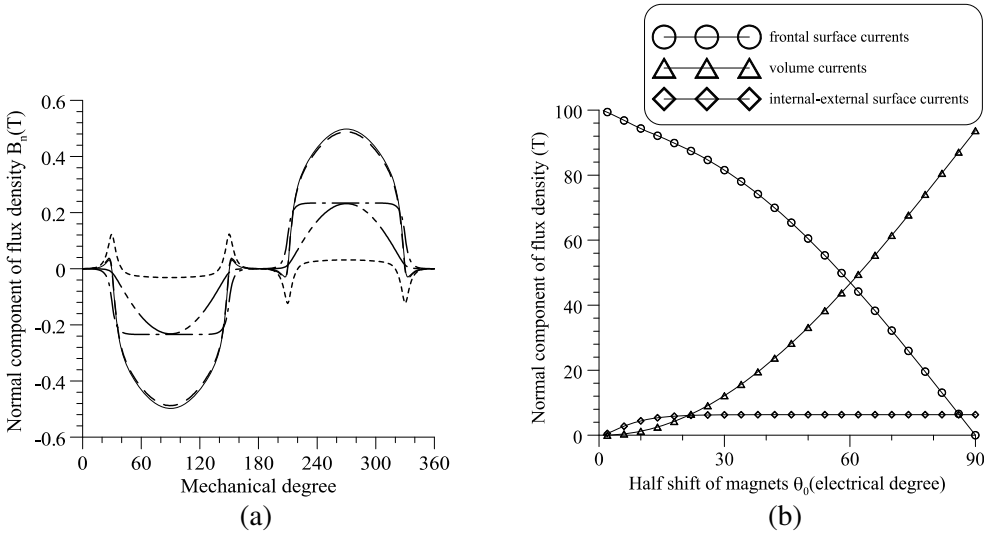

Figure 11. Bipolar machine with 2/3 shift of permanent magnets $\theta_0 = 60°$ ($n_b = 1$). (a) Contribution for a 60° electrical degree half shift (—— analytical model) and (– – – finite elements model), — - — - — volume currents contribution, — - - — - - frontal surface currents contribution, - - - - - - internal-external currents surface contribution. (b) 2-pole machine with variable shift of permanent magnets: related value of contributed flux densities induced by all types of equivalent currents.

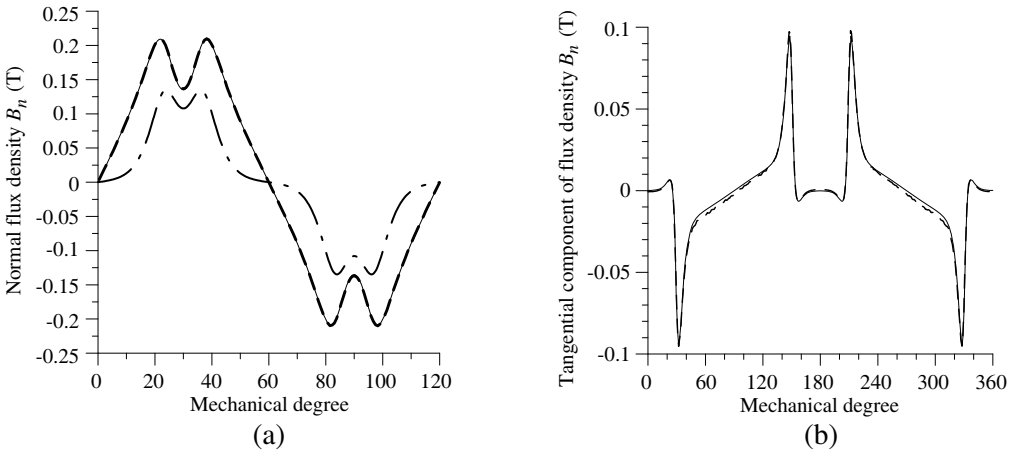

Figure 12. Bipolar machine permanent magnets 60° shift for tangential parallel permanent magnets (—— analytical model) and (– – – finite elements model). (a) Normal flux density component (— - — for classical model). (b) Tangential flux density component.

is increased, opposite to frontal surface currents contribution. They have same values for a 60° electrical shifted permanent magnet ($\theta_0 = 60°$). It is important to notice that volume currents contributions are small for small magnet bars. Their contribution is less than 1% for $\theta_0 = 9°$.

For internal-external surface currents, the contribution is about 6% for $\theta_0 > 19°$ and less than 1% for $\theta_0 < 2°$.

For segmented permanent magnets, we note that classical model give practically the same results as the proposed model for $\theta_0 < 5°$ (with 2% maximum difference in maximal value of normal flux density). The classical model is then available for segmented permanent magnets with thin bars.

In Fig. 12 we can see other analytical-FEMM comparison for tangential parallel magnetized permanent magnets in the structure of 60° half shift. A good correlation is noted between these results. We can see that classical model is very insufficient for this type of permanent magnet and needs to take into account the volume currents.

This type of magnetization cannot be applied alone on surface mounted permanent magnet machines. It can be used, for example, in Halbach structures.

7. MODEL VALIDATION

The proposed model is valid for the studied structure. But, is it also valid for other structures (with different radius r_o and r_i)? If ratios r_i/r_a and r_o/r_a are respected, the measurement value of r_a does not affect magnetic results (such flux densities) of structures. In the following, we consider structures with constant radius r_a, but we change two parameters:

- h: permanent magnets height: $h = (r_o - r_i)$.
- a: mechanical air gap: $a = (r_a - r_o)$.
- $n_b = 2$ (there are two bars under each pole).

In Fig. 13, we can see the maximum value of normal component of flux density $Bn_{\max}$ for different structures. Results are obtained with both methods: analytical and FEMM.

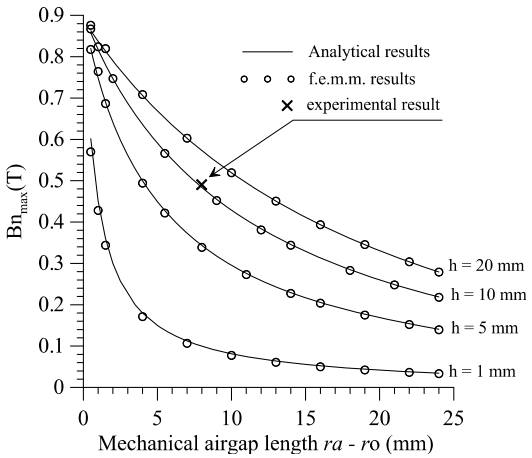

Figure 13. Maximal value of normal component of flux density in the middle of mechanical air gap for different values of air gap and permanent magnets height.

The two methods gave similar results for all these structures. We can then conclude that the proposed model of segmented parallel permanent magnets is verified.

In Fig. 14, we can see radial and tangential components of flux densities obtained for the two extreme structures chosen for this validation. The first structure cr1 has a thin magnetic air gap ($h = 1\,\text{mm}$, $a = 1\,\text{mm}$), and the second structure cr2 has a large magnetic airgap ($h = 20\,\text{mm}$, $a = 25\,\text{mm}$).

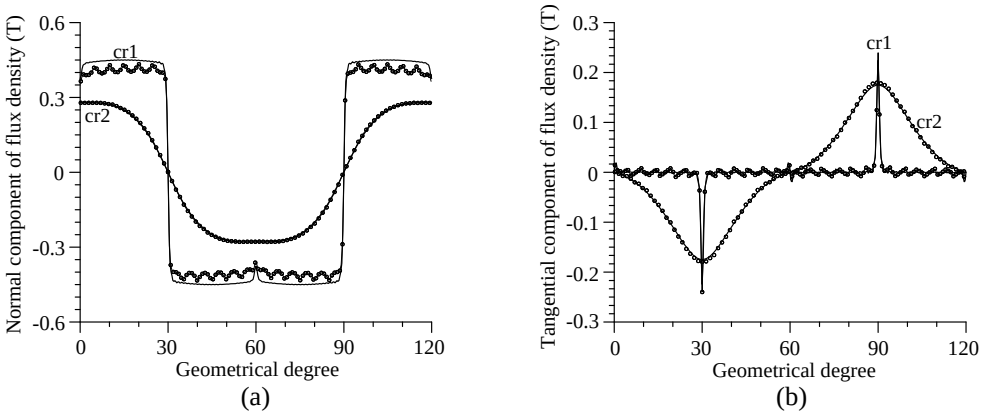

Figure 14. Analytical (—) and FEMM (□□□□) flux density distribution for thin (cr1) and large (cr2) magnetic air gap. (a) Normal component. (b) Tangential component.

8. HARMONIC ANALYSIS

The solutions of Equations (53) and (54) give a complete expression of the magnetic potential in the mechanical air gap in the case of radial parallel magnet bars as follows:

$$A = \sum_n M_0 \frac{r_m}{\pi} \frac{\left(n\left(1 - ch\left(n \ln\left(\frac{r_o}{r_i}\right)\right)\right) - sh\left(n \ln\left(\frac{r_a}{r_o}\right)\right)\right)}{2n^2 sh\left(n\left(\ln\frac{r_a}{r_o} + \ln\frac{r_o}{r_i}\right)\right)} \left(\left(\frac{r}{r_a}\right)^n + \left(\frac{r_a}{r}\right)^n\right) S_n \sin(n\theta) \tag{59}$$

$$S_n = \begin{cases} \cos\theta_i \left(2\alpha\theta_b - \sin(2\alpha\theta_b)\right) & n = 1 \\ 2p\cos(n\theta_i)\left(\dfrac{\sin(n-1)\alpha\theta_b}{(n-1)} - \dfrac{\sin(n+1)\alpha\theta_b}{(n+1)}\right) & n \neq 1 \end{cases}$$

As we can see from Equation (59), the potential is the sum of harmonic terms in $\sin(n\theta)$.

9. PARALLEPIPED BARS

In following, we can see results of the equivalent analytical model and the comparison with finite elements results for the last proposed model: the parallepiped bars.

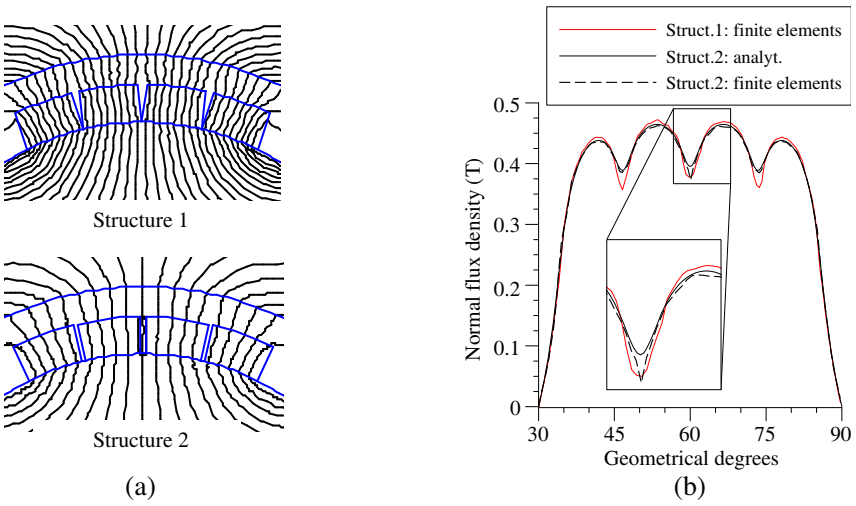

Figure 15. Analytical and numerical results for real and equivalent models of radial parallel segmented magnet bars. (a) Flux density lines. (b) Normal component of flux density.

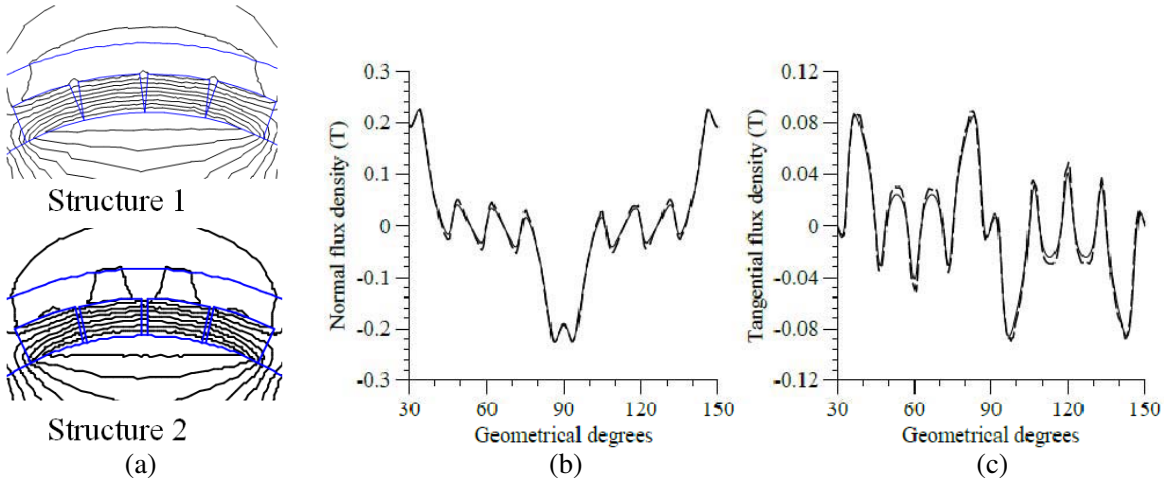

Figure 16. Analytical and numerical results for real and equivalent models of tangential parallel segmented magnet bars. (a) Flux density lines. (b) Normal component of flux density. (c) Tangential component. – – – Numerical results for real structure (structure 1). —— Analytical results for equivalent structure (structure 2).

In Fig. 15, we can see the two studied structures. For the real structure, we have numerical results, and for the equivalent structure, we have both analytical and numerical results.

The model is applied to a six poles synchronous machine, with an angular shift of 80 electrical degrees and four (04) magnets by pole.

The developed model is applied to tangential parallel magnetization parallepiped segmented bars. In Fig. 16, we can see parallel magnetization potential contours for the two structures: true and its equivalent model. Radial and tangential components are shown. These results (analytical and numerical) conform, and we can deduce that the presented analytical model is as close as possible to the real structure for slotless surface permanent magnets machines.

10. CONCLUSION

In this paper, we have presented a complete model of permanent magnets in real magnetization (in parallel direction) for two types of polarizations: radial and tangential.

For complete surface currents models, we have completed classical models by introducing equivalent volume currents. It is the originality of this work.

The model obtained is compared to free code finite element method (FEMM [30]) results, and a good convergence is noted. Experimental results also validates our model in some special cases.

In all cases, the model is reliable and gives very good results compared to the numerical method. We noted in our study the balance of volume currents in the case of large aperture magnets. These currents begin to disappear in thin magnets, as we can see in Fig. 12. The classical model is valid for parallel magnetization when the shift of magnets is less than 10 electrical degrees. This model can be extended to rotating magnetization, and it is an ideal tool to design parallel magnet bars.

We have extended our model to segmented magnet bars and separated magnet bars. Results are also excellent in both cases of parallel magnetization: radial and tangential.

We finally tried to approach the true geometry of the magnets giving them a parallelepiped, which is done by considering tile magnets equivalent. Results obtained by this approach are satisfactory. The model thus developed can be extended to the calculation of magnetization and rotating Halbach structures.

In other way, the obtained expressions of potential magnetic are easy for calculate back EMF and torque.

REFERENCES

1. Warnick, K. F. and P. H. Russer, "Differential forms and electromagnetic field theory," *Progress In Electromagnetics Research*, Vol. 148, 83–112, 2014.
2. Mahmoudi, A., S. Kahourzade, N. A. Rahim, H. W. Ping, and N. F. Ershad, "Slot-less torus solid-rotor-ringed line-start axial-flux permanent-magnet motor," *Progress In Electromagnetics Research*, Vol. 131, 331–355, 2012.
3. Chen, M., K.-T. Chau, C. H. T. Lee, and C. Liu, "Design and analysis of a new axial-field magnetic variable gear using pole-changing permanent magnets," *Progress In Electromagnetics Research*, Vol. 153, 23–32, 2015.
4. Rahideha, A. and T. Korakianitis, "Analytical calculation of open-circuit magnetic field distribution of slotless brushless PM machines," *Intern. Journ. of Electrical Power & Energy Systems*, Vol. 44, No. 1, 99–114, Jan. 2013.
5. Tiegna, H., Y. Amara, and G. Barakat, "Overview of analytical models of permanent magnet electrical machines for analysis and design purposes," *Mathematics and Computers in Simulation*, Vol. 90, 162–177, 2013.
6. Boules, N., "Prediction of no load flux density distribution in permanent magnet machines," *IEEE Trans. on Ind. Appl.*, Vol. 21, 633–643, Jul.–Aug. 1985.
7. Zhu, Z. Q., D. Howe, and C. C. Chan, "Improved analytical model for predicting the magnetic field distribution in brushless permanent magnet machines," *IEEE Trans. on Magnetics*, Vol. 38, No. 1, 229–238, Jan. 2002.
8. Dubas, F. and C. Espanet, "Analytical solution of the magnetic field in permanent-magnet motors taking into account slotting effect: No-load vector potential and flux density calculation," *IEEE Trans. on Magnetics*, Vol. 45, No. 5, 2097–2109, May 2009.
9. Holm, S. R., H. Polinder, and J. A. Ferreira, "Analytical modeling of a permanent-magnet synchronous machine in a flywheel," *IEEE Trans. on Magnetics*, Vol. 43, No. 5, May 2007.
10. Boughrara, K., D. Zarko, R. Ibtiouen, O. Touhami, and A. Rezzoug, "Magnetic field analysis of inset and surface mounted permanent magnet synchronous motors using Schwarz-Christoffel transformation," *IEEE Trans. on Magnetics*, Vol. 45, No. 8, 3166–3178, Aug. 2009.
11. Chikouche, B. L., K. Boughrara, and R. Ibtiouen, "Cogging torque minimization of surface-mounted permanent magnet synchronous machines using hybrid magnet shapes," *Progress In Electromagnetics Research B*, Vol. 62, 49–61, 2015.
12. Ravaud, R., G. Lemarquand, and V. Lemarquand, "Magnetic field created by a uniformly magnetized tile permanent magnet," *Progress In Electromagnetics Research B*, Vol. 24, 17–32, 2010.
13. Bellara, A., Y. Amara, G. Barakat, and B. Dakyo, "Two-dimensional exact analytical solution of armature reaction field in slotted surface mounted PM radial flux synchronous machines," *IEEE Trans. on Magnetics*, Vol. 45, No. 10, 4534–4538, Oct. 2009.
14. Lubin, T., S. Mezani, and A. Rezzoug, "Exact analytical method for magnetic field computation in the air-gap of cylindrical electrical machines considering slotting effects," *IEEE Trans. on Magnetics*, Vol. 46, No. 4, 1092–1099, Apr. 2010.
15. Holm, S. R., H. Polinder, and J. A. Ferreira, "Analytical modeling of a permanent-magnet synchronous machine in a flywheel," *IEEE Trans. on Magnetics*, Vol. 43, No. 5, May 2007.
16. Gysen, B. L. J., K. J. Meessen, J. J. H. Paulides, and E. A. Lomonova, "General formulation of the electromagnetic field distribution in machines and devices using Fourier analysis," *IEEE Trans. on Magnetics*, Vol. 46, No. 1, 39–52, Jan. 2010.
17. Lubin, T., S. Mezani, and A. Rezzoug, "Two-dimensional analytical calculation of magnetic field and electromagnetic torque for surface-inset permanent-magnet motors," *IEEE Trans. on Magnetics*, Vol. 48, No. 6, 2080–2091, Jun. 2012.
18. Li, W. and K.-T. Chau, "Analytical field calculation for linear tubular magnetic gears using equivalent anisotropic magnetic permeability," *Progress In Electromagnetics Research*, Vol. 127, 155–171, 2012.

19. Yan, L., L. Zhang, T. Wang, Z. Jiao, C.-Y. Chen, and I.-M. Chen, "Magnetic field of tubular linear machines with dual halbach array," *Progress In Electromagnetics Research*, Vol. 136, 283–299, 2013.
20. Rasmussen, K. F., "Analytical prediction of magnetic field from surface mounted permanent magnet motor," *Proc. IEEE IEMDC*, Seattle, WA, May 9–12, 1999.
21. Boutora, Y., R. Ibtiouen, and N. Takorabet, "Analytical model of magnet bars of surface permanent magnet slotless machine," *13th International Conference on Electrical Machines, ICEM 2012*, 2772–2778, Marseille, Sep. 4–6, 2012.
22. Nogarede, B., "Etude de moteurs sans encoches à aimants permanents de forte puissance à faible vitesse," Doctorat. Thesis, INP Toulouse, France, 1990.
23. Nogarede, B., M. Lajoie-Mazenc, and B. Davat, "Modélisation analytique des machines à aimants à induit sans encoches," *Revue de Physique Appliquée*, No. 25, 707–720, Paris, 1990.
24. Zhu, Z. Q., L. J. Wu, and Z. P. Xia, "An accurate subdomain model for magnetic field computation in slotted surface-mounted permanent magnet machines," *IEEE Trans. on Magnetics*, Vol. 46, No. 4, 1100–1115, Apr. 2010.
25. Bentouati, S., Z. Q. Zhu, and D. Howe, "Influence of design parameters on the starting torque of a single-phase PM brushless DC motor," *IEEE Trans. on Magnetics*, Vol. 36, No. 5, 3533–3536, May 2000.
26. Jung, J.-W. and T. H. Kim, "A study on the effect of the magnetization direction on the iron loss characteristics in brushless DC motors," *Journal of Magnetics*, Vol. 15, No. 1, 40–44, 2010.
27. Ferraris, L., P. Ferraris, E. Pošković, and A. Tenconi, "Evaluation of the magnetization direction effects on ferrite PM brushless fractional machines," *IECON 2012, 38th Ann. Conf. on IEEE Indust. Electron. Society*, 6194–6199, Alessandria, Italy, Oct. 25–28, 2012.
28. Ferraris, L., P. Ferraris, E. Pošković, and A. Tenconi, "Comparison between parallel and radial magnetization in PM fractional machines," *IECON 2011, 37th Ann. Conf. on IEEE Indust. Electron. Society*, 1776–1782, Turin, Italy, Nov. 7–10, 2011.
29. Jang, S.-M., H.-I. Park, J.-Y. Choi, K.-J. Ko, and S.-H. Lee, "Magnet pole shape design of permanent magnet machine for minimization of torque ripple based on electromagnetic field theory," *IEEE Trans. on Magnetics*, Vol. 47, No. 10, 3586–3589, Oct. 2011.
30. Meeker, D., "Manual of femm4.2," available http://www.femm.info/wiki/HomePage.